UNIVERSITY OF AMSTERDAM

UvA-DARE (Digital Academic Repository)

Angle-resolved cathodoluminescence nanoscopy

Coenen, T.

Publication date
2014

Link to publication

Citation for published version (APA):
Coenen, T. (2014). *Angle-resolved cathodoluminescence nanoscopy*. [Thesis, externally prepared, Universiteit van Amsterdam].

General rights
It is not permitted to download or to forward/distribute the text or part of it without the consent of the author(s) and/or copyright holder(s), other than for strictly personal, individual use, unless the work is under an open content license (like Creative Commons).

Disclaimer/Complaints regulations
If you believe that digital publication of certain material infringes any of your rights or (privacy) interests, please let the Library know, stating your reasons. In case of a legitimate complaint, the Library will make the material inaccessible and/or remove it from the website. Please Ask the Library: https://uba.uva.nl/en/contact, or a letter to: Library of the University of Amsterdam, Secretariat, P.O. Box 19185, 1000 GD Amsterdam, The Netherlands. You will be contacted as soon as possible.

UvA-DARE is a service provided by the library of the University of Amsterdam (https://dare.uva.nl)

Download date:04 Nov 2026

2

Spectroscopy with fast free electrons

Electron beam spectroscopies provide a powerful platform for studying a wide variety of nanophotonic structures like nanoantennas, nanocavities, and photonic crystals. In this Chapter we describe in detail which processes occur when a fast electron beam interacts with a sample. Furthermore we discuss the experimental techniques that are used throughout this thesis. In particular we describe angle-resolved cathodoluminescence imaging spectroscopy and electron energy-loss spectroscopy. Both techniques rely on a beam of energetic free electrons as excitation source but use different detection mechanisms.

2.1 Electron beam excitation

When a beam of energetic fast electrons (0.1 keV – 300 keV of energy per electron) hits a sample a multitude of processes can occur. The interaction with the sample leads to the generation of low-energy secondary electrons (SEs) and more energetic backscattered electrons (BSEs) which provide information about the surface topology and composition of the sample and hence can be used for microscopy. Electrons that are transmitted either directly or indirectly can be used for microscopy as well. Because electrons have a restmass their de Broglie wavelength is orders of magnitude smaller than the wavelength for photons at the same energy. For a 2 eV electron the corresponding wavelength is 0.86 nm whereas for a photon it is 620 nm. At 300 keV an electron travels at $0.8c$ and relativistic effects must be taken

into account; The de Broglie wavelength then is 2 pm. Even though state-of-the-art electron microscopes still operate far away from the electron wave diffraction limit, an imaging resolution of 80 pm has been demonstrated which means that structure and composition of materials can be studied on the atomic scale [75–77].

Besides the electron signals, a broad spectrum of electromagnetic radiation ranging from x-rays to the mid-IR is generated through a variety of incoherent and coherent processes which will be discussed below. The electromagnetic radiation that is generated in the visible/NIR regime of the spectrum is usually referred to as cathodoluminescence (CL) as the radiation is generated by cathode rays (fast electrons). For an historical overview on the discovery of cathode rays and CL we refer the reader to Ref. [78]. Figure 2.1 shows an overview of signals that can be measured when a material is irradiated by energetic electrons, together with the corresponding characterization techniques.

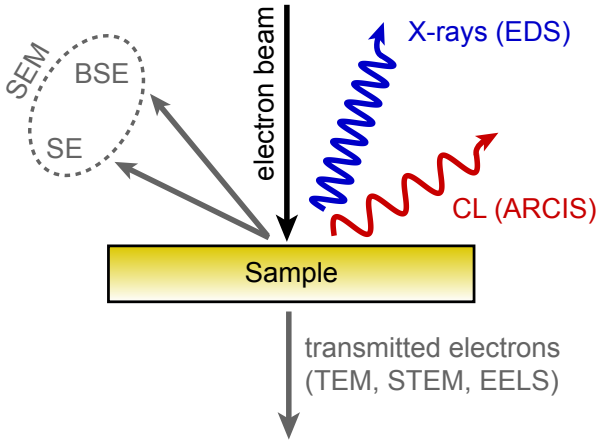


Figure 2.1: Schematic showing some of the processes that occur when an energetic beam of electrons impinges on a sample. These processes are used for different characterization techniques as indicated in the schematic.

2.1.1 Coherent excitation

An electron moving at a constant velocity through space is accompanied by evanescent electromagnetic fields that extend away from the electron and cannot couple to propagating radiation [63]. When the electron interacts with matter these fields can be coherently transferred and sometimes converted to free-space radiation. An example of such a process is transition radiation (TR) generation, where an electron passes through an interface between two media with different refractive indices. The electron transition through the interface polarizes electrons near the interface, inducing an effective vertical dipole moment. Because the electron tran-

sition is very fast the TR spectrum is broad band. Furthermore, the interaction is highly localized in space which means there is a broad distribution in available momenta. This allows direct excitation of guided waves that have in-plane momenta larger than that of free-space light at the same frequency, such as surface plasmon polaritons (SPPs) on the interface between a plasmonic metal and a dielectric. A schematic of TR and SPP excitation for an Au substrate is shown in Fig. 2.2(a).

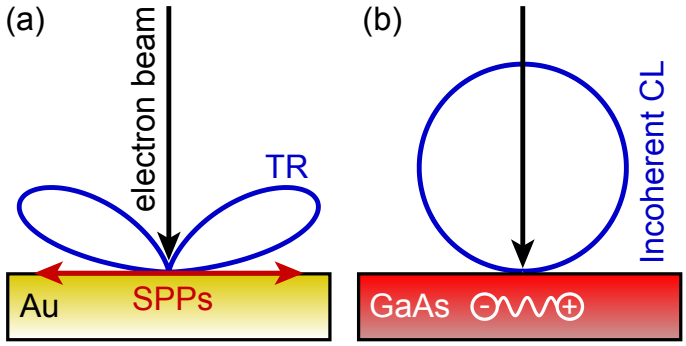


Figure 2.2: (a) Excitation of a gold substrate where transition radiation and SPPs are generated. The blue curve represents the radiation pattern for TR which is similar to that of a vertical point dipole source on a gold substrate (for a detailed description of how this pattern is calculated see Section 3.3). (b) Schematic of electron beam excitation of gallium arsenide where radiative electron hole pair recombination lead to a strong incoherent CL component. Due to the randomized emission inside of the substrate the emission pattern usually resembles a Lambertian emission distribution.

A second example of coherent excitation is Cherenkov radiation where the electron travels faster than the speed of light in the medium, which means that the electron dispersion lies above the light line in the medium and the evanescent fields transform into radiating fields at an angle that is determined by the velocity of the the electron relative to the speed of light in the medium. It has been proposed that this type of radiation can be utilized for efficient heralded single-photon generation of a particular color, if one lets the electrons move parallel to a 1D waveguide [79].

The probability of an electron losing energy through these coherent processes can be related to the induced vertical electric field acting back on the electron. The electron is sensitive only to the vertical electric field component because that is the only way in which the electron can decelerate and perform work, *i.e.* transfer energy to a structure. Because of energy conservation the electron can only loose energy to a structure. However, if an external field is supplied such as an ultrafast laser pulse for example, the electrons can also gain quanta of energy [80–83]. Because of this E_z sensitivity the electrons often couple to vertical electric dipole modes and guided modes with transverse magnetic (TM) character like the single-interface SPP mode in Fig. 2.2. This is markedly different from plane waves where the electric field

oscillates transverse to the propagation direction leading to a preferential coupling to xy-components for normal incidence.

It has been shown theoretically that for z-invariant structures there exists a rigorous connection between the electron energy-loss (EEL) probability and the z-projection of the local density of optical states (LDOS) integrated along the electron trajectory [63, 84]. Also for structures that do not have a z-invariant geometry there can be qualitative agreement between the z-projection of the integrated LDOS and the EEL signal although this is not always the case, as is described in Ref. [85]. The EEL probability takes into account non-radiative as well as radiative processes whereas the CL probability contains information only about the radiative processes. This means that modes that are dark, *i.e.* that do not couple to far field radiation, as bulk plasmons for example, do show up in the EEL but not in the CL signal. Making quantitative predictions about the LDOS based on the EEL/CL probability is not straightforward and one should be cautious in doing so. As the electron beam is not affected by xy LDOS components, optical modes with strong in-plane fields such as dipolar dimer modes which exhibit strong hotspots in the dimer gap do not appear as such in EEL/CL maps [85–88]. Nevertheless, using coherent electron beam excitation one can obtain useful insights into the local optical response of nanostructures for a broad wavelength range simultaneously. By using a pulsed electron source in conjunction with a femtosecond laser one can also study the time dynamics of light-electron interactions in nanostructures which is also referred to as 4D electron microscopy (2 spatial dimensions, energy, and time) [81, 83, 89–91]. Furthermore, by rotating a sample one can perform tomography and holography on nanomaterials which can be used to obtain structural and chemical information in 3D [25]. Most recently, EELS and CL tomography have been developed demonstrating yet another form of 4D electron microscopy, as these techniques provide 3D spatial information on the local optical properties for a broad range of energies [92–94].

2.1.2 Incoherent excitation

Besides the coherent processes electrons can also excite incoherent transitions in a material. In particular, one can drive high-energy core transitions which can be detected using EELS (see Section 2.5) or energy-dispersive x-ray spectroscopy (EDS). These transitions provide a unique fingerprint for local elemental analysis in electron microscopy. Incoherent light emission in the visible/near-infrared regime can also occur through band-edge electron-hole recombination in bulk/nanostructured semiconductors [95, 96] and quantum-confined structures [70, 97], intra-$4f$ transitions in rare-earth ions, defect luminescence in materials [98, 99] *etc.* This incoherent emission has been used in the past in cathode-ray-tube (CRT) televisions, and is still used in geology to identify and characterize minerals [100]. Furthermore, phosphor screens are used routinely in electron microscopes to convert electron signals into optical signals as these are easier to detect using standard silicon cameras or photomultiplier

tubes. It is important to note that the cathodoluminescence spectrum does not necessarily match the photoluminescence spectrum of a material because the relatively large momentum of the electrons allows for the excitation of transitions which are momentum-forbidden for light. Also, the cross sections for electron impact excitation generally differ from those for optical excitation. Nevertheless incoherent CL spectroscopy provides a powerful platform for locally studying the material properties. Figure 2.3 shows spectra that we have measured on SiO_2:Er^{3+}, InP, GaAs, SiO_2, YAG:Ce^{3+}, CdS, InGaN, ZnO, and GaN respectively. The strong emission peaks that are observed are due to one or more of the incoherent processes mentioned above.

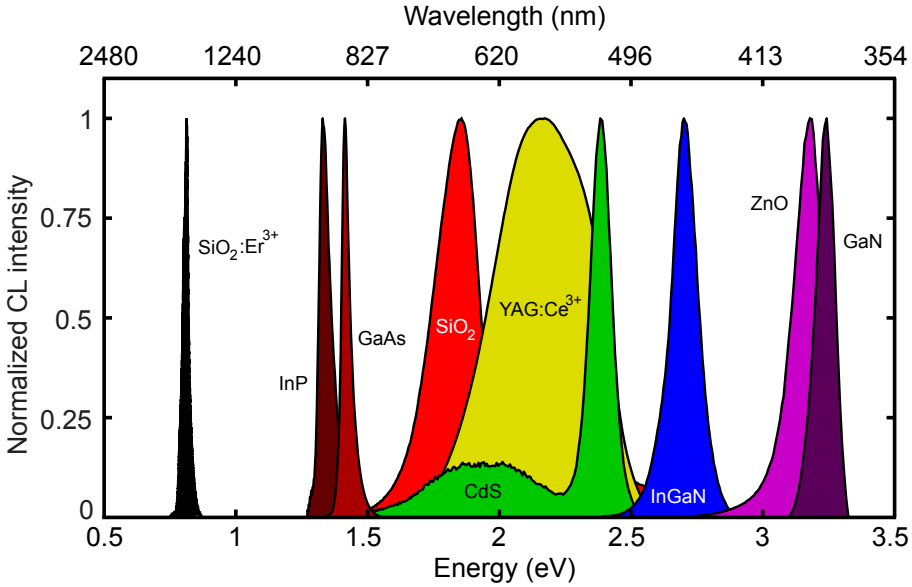


Figure 2.3: Normalized CL spectra (5 – 30 keV electrons) for a variety of dielectric and semiconductor materials. The SiO_2:Er^{3+}, GaAs, SiO_2, YAG:Ce^{3+}, and GaN emission was measured on bulk/planar materials. The other spectra were measured on nanomaterials: InP (nanowire grown with the vapor-liquid-solid method), CdS (colloidal platelet), InGaN (quantum wel embedded in GaN), and ZnO (nanoparticle powder).

Because an electron beam can be tightly focused, precise lateral characterization of materials is possible. By changing the electron energy one can also alter the penetration depth enabling materials characterization in 3D. Incoherent emission is generally oriented randomly inside the material and as result it is emitted approximately in a Lambertian emission distribution [101, 102]. A schematic of this process is shown in Fig. 2.2(b) for GaAs which is a strongly luminescent material due to its direct bandgap. Note that there is also TR radiation generation for GaAs but its

intensity is very small compared to the incoherent band edge luminescence. The excitation of incoherent radiation can be very efficient because one energetic electron can easily create multiple photons as it creates a cascade of excitation events. In fact, incoherent luminescence is usually excited more efficiently by the cloud of slow secondary electrons rather than the primary beam. As a result the incoherent radiation often is much stronger than the coherent radiation from the same structure. This puts restrictions on the substrates that can be used if one is interested in coherent signals. For instance, SiO_2 which is a standard substrate for many optical experiments, exhibits very strong defect luminescence under electron beam irradiance [98] (see Fig. 2.3) making it impractical for coherent CL spectroscopy. Finally, it should be noted that in some cases the incoherent CL is bleached. This can be particularly severe for organic compounds which often decompose under electron irradiation.

2.2 Angle-resolved cathodoluminescence imaging spectroscopy

In this section we will discuss the angle-resolved cathodoluminescence imaging spectroscopy (ARCIS) setup that is used throughout this thesis. The main component of the setup is a FEI XL-30 Schottky field emission gun (SFEG) scanning electron microscope (SEM) (see Fig. 2.4(a)). The SEM is equipped with a specially designed micromanipulation stage that carries an off-axis aluminum paraboloid mirror (0.1 parabola coefficient, 0.5 mm focal distance, 1.46π sr acceptance angle, 10 nm RMS roughness, and $\lambda/2$ curve accuracy)(Fig. 2.4(b,c)). Directly above its focal point, this paraboloid has a 600-μm-diameter hole through which the electron beam can reach the sample. The size of the hole is a tradeoff between loss in acceptance angle and a larger field of view in the electron microscope as the hole size is increased. The mirror collects the generated CL and redirects it out of the SEM through a glass vacuum flange into an enclosed optics box (the black box in Fig. 2.4(a)). The nanomanipulation stage allows proper focusing of the paraboloid by using four piezoelectric stepper motors connected to a titanium leaf spring system (visible in Fig. 2.4(b)). This system provides translational degrees of freedom (x, y over a range of ~1 mm with an accuracy of ~500 nm) as well as control over mirror tilt and yaw (~10° range with an accuracy of ~0.1°). Vertical alignment of the sample with the mirror focus is achieved by varying the SEM stage height. The alignment procedure is discussed in more detail in Section 2.3. The micropositioning system was designed by Iliya Cerjak and Hans Zeijlemaker at AMOLF.

Figure 2.4(d) shows a schematic of the CL setup. For spectral imaging purposes, the CL that is collected by the paraboloid is focused onto a 600-μm-diameter-core multimode fiber using an achromatic lens. This fiber diameter gives the system an effective focal area of 20×20 μm^2. Outside this area the the CL-emission is not efficiently collected by the fiber. The fiber is connected to a spectrometer (PI Acton SP2300i) with a liquid-nitrogen-cooled (LN) silicon CCD array (Princeton In-

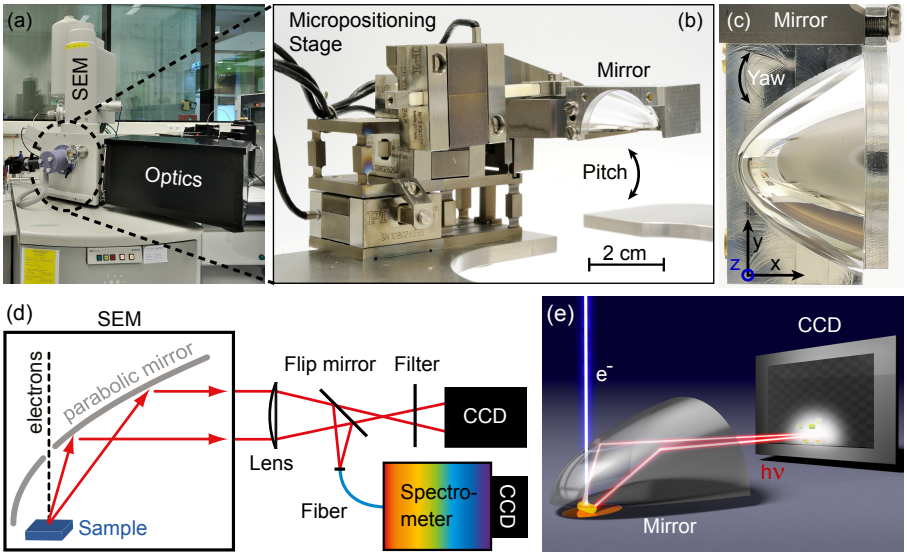


Figure 2.4: (a) Photograph of FEI XL-30 SFEG with CL optics box attached. (b) Inside the chamber a piezoelectric mirror positioning system is mounted which can used to position a parabolic mirror in four dimensions (x,y, pitch, and yaw). (c) Photograph taken from the bottom of the mirror. (d) Schematic overview of the setup showing the different detection schemes. (e) Graphical representation of angle-resolved detection of CL on a 2D CCD array (image by Tremani). (Design in (b) by Iliya Cerjak and Hans Zeijlemaker, pictures in (a-c) by Henk-Jan Boluijt)

struments, Spec-10 100F/LN, 1340 × 100 pixels) which is used for spectral analysis of the CL emission. For all spectral measurements shown throughout this thesis we have used hardware binning of the CCD pixels for a better signal-to-noise ratio (SNR)(100 times in the vertical direction and 4 times in the horizontal direction yielding an effective imaging array of 335 × 1 pixels). A spectrometer with a 1 × 1024 pixel LN-cooled InGaAs photodiode array for measurements in the infrared (900 – 1650 nm) (PI OMA V 1.7) is also available for CL experiments in the near-infrared. Data taken with this IR system are not reported in this thesis.

2.2.1 Spectral imaging

By raster-scanning the tightly focused electron beam in 2D we can build up a 3D datacube by collecting a spectrum at each excitation position. At each position we can also collect the secondary electron signal so we can simultaneously collect a SEM image so that CL features can be correlated with geometrical features. We should note that the SEM images that are collected during CL sessions are of lower quality than for a regular sample inspection in a SEM, due to the presence of the parabolic mirror. First, the mirror prevents the sample from reaching the optimum

distance from the pole piece for imaging (sample can only get to 13 mm whereas 5 mm is optimal). This, and the disturbing effect of the large metallic mirror in between pole piece and sample precludes the use of the ultra-high resolution immersion mode in which a large magnetic field is applied to the sample to direct electrons towards the through-the-lens electron detector. Second, the metallic mirror also perturbs the focusing fields of the electromagnetic lenses, reducing the imaging resolution. Third, the mirror blocks a large part of the secondary electrons preventing them from reaching the detector, thereby greatly reducing the SE signal. In fact, due to the geometry of our SEM the SE detector is behind the parabolic mirror (on the closed side of the mirror) which is suboptimal. The collection efficiency could be enhanced by having the SE detector on the open side of the mirror. These issues reduce the SE imaging resolution to ~5 – 10 nm which is good enough for many optical studies. Even though only a fraction of the SEs are collected, the SNR in the images is still good enough because we typically use a beam current of ~1 nA which is 10 – 100 times higher than for regular SEM imaging.

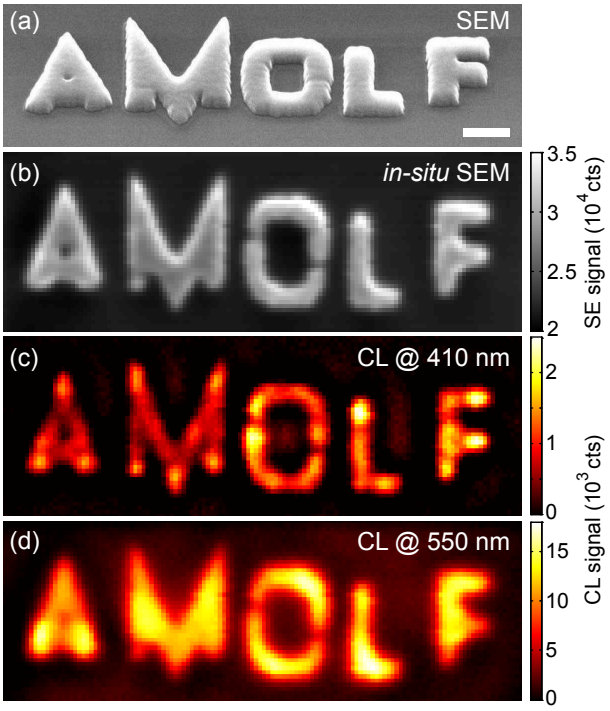


Figure 2.5: (a) High-resolution scanning electron micrograph of an AMOLF logo etched into a 100 nm thick Si layer on a 300 nm box layer of SiO_2, taken at a 52° stage tilt (scale bar corresponds to 250 nm). (b) Secondary electron signal collected during CL acquisition. 2D CL excitation maps of the structure at (c) λ_0 = 410 nm and (d) 550 nm integrated over a 20 nm bandwidth.

In order to reliably scan a structure we use a drift-correction algorithm which compares SEM images of an area with a clear geometrical feature to correct for the effects of beam-and sample drift *in situ*. To minimize charging effects it is important to use a reasonably conductive substrate (metals, semiconductors, or thin insulators layers with conductive substrate). Electron-transparent Si_3N_4 or amorphous carbon TEM membranes haven been employed successfully as well.

An example of a 2D spectral imaging measurement is shown in Fig. 2.5(c,d) for free space wavelengths of 410 and 550 nm respectively, together with a scanning electron micrograph of the structure taken at high resolution (a) and the SE image that was collected simultaneously during the CL scan (b). The structure on which the measurement was performed was an AMOLF logo etched into a 100 nm thick silicon device layer of an SOI wafer with reactive-ion etching (same fabrication procedure as described in Section 12.2). Because the feature size of the characters is on the scale of the wavelength in silicon, optical resonances exist in this logo which can be visualized with CL imaging. The scanning pixel size in this measurement was 20 nm × 20 nm and we used an integration time of 0.2 s/pixel at an 1 nA beam current. The total measurement time was 20 minutes for this scan. The background signal from the underlying oxide layer and silicon substrate were subtracted to visualize the modes in the logo. The excitation distributions clearly depend on wavelength which is expected for such resonant structures as will be discussed in Chapter 12.

2.2.2 Measuring angular emission profiles

Besides the spectral response, knowledge of the angular emission profile of a nanostructure provides key information about the optical modes and band structure of a nanomaterial. The 2D lateral intensity profile of the parallel beam emanating from the paraboloid mirror is a direct measure of the angular emission. We measure the beam profile by directing it to a 2D Peltier-cooled (-70°C) back-illuminated CCD array (Princeton Instruments, PIXIS 1024B with a 1024 × 1024 pixel CCD chip). A schematic illustration of this type measurement is shown in Fig. 2.4(e). The achromatic lens is defocused to ensure that the beam fills the CCD array (demagnification factor of 2). This collection geometry is similar to "Fourier imaging", also known as "conoscopic imaging", or "defocused imaging" in microscopy [103, 104]. Such Fourier imaging consists of imaging the back-aperture of a microscope objective that contains the full wave vector information of emitted light onto a CCD. For this setup, the equivalent interpretation is that each point on the paraboloid is associated with a unique emission angle which can be described by a zenithal angle θ running from 0° to 90° (where $\theta = 0°$ is normal to the surface) and an azimuthal angle ϕ running from 0° to 360° (where the paraboloid vertex is at $\phi = 180°$). If the mirror is well-focused, each point in the CCD image corresponds to a single point on the paraboloid and as a result we can directly convert a CCD image to a radiation pattern for the upper hemisphere. Because of the mirror curvature the amount of solid angle collected per CCD pixel is not constant and the data points in θ and ϕ are not equally spaced. We use a triangular interpolation

routine to obtain an equidistant data set in θ and ϕ space, and we correct the data for the coordinate transformation to obtain emitted power per steradian (for details about the conversion from CCD image to angular pattern see Chapter 3). For the angular measurements we usually use 4 × 4 hardware binning of the CCD pixels for an improved SNR. For spectral selectivity 40 nm band pass color filters are used, which represents a good trade-off between spectral resolution and signal level. We use an electric flip mirror to switch between the spectral and angular functionalities of the CL setup.

In the beam path space is reserved for other optical components such as polarizers. Polarization-sensitive angle-resolved CL is discussed in detail in Chapter 6. A commercial version of our ARCIS system has been developed recently by DELMIC B.V. A full description and a 3D movie of that system can be found at www.delmic.com/products/sparc/.

2.3 Mirror alignment

Accurate alignment of the parabolic mirror is key for efficient CL spectroscopy. The piezodriven micropositioning system allows accurate positioning of the mirror such that the electron beam hits the sample exactly in the mirror focus. If the mirror is aligned properly, the beam emanating from the mirror should have a semicircular shape similar to that of the mirror end facet. However, if there is a misalignment in x,y, or z (see coordinate system in Fig. 2.4(c)) the beam pattern is distorted in a way characteristic for that misalignment. Using raytracing calculations one can calculate what type of pattern should be expected for a given misalignment [105]. Figure 2.6 shows the effect of a misalignment in x, y, and z on the beam profile, both measured and calculated using raytracing. The pattern for the fully aligned mirror is shown in the top left image of Fig.2.6. The measured images are taken without the lens flipped in, *i.e.* without demagnification, because in this configuration misalignments can be recognized an corrected more easily.

While the raytracing program uses absolute displacements in x,y, and z with respect to the ideal mirror focus position, the piezomotors do not give position feedback so do not provide absolute values for the mirror position. Actual misalignments for x and y in the experiment were derived by matching the raytracing pattern to the measured pattern for a given misalignment, and are given in each set of images (misalignment values are given relative to the mirror focus position). The SEM stage does have absolute position feedback so for z the measured stage positions are used as input for the raytracing program. Overall there is good agreement between the raytracing and the measured patterns, both in the pattern shape and asymmetry. The differences are explained by imperfections in the mirror due to the diamond turning fabrication process (clearly visible as radial distortions in the measured images), and small differences in pitch and yaw angle, which are assumed to be zero in the raytracing program and the experiment.

During the mirror alignment we can recognize the distorted patterns and move

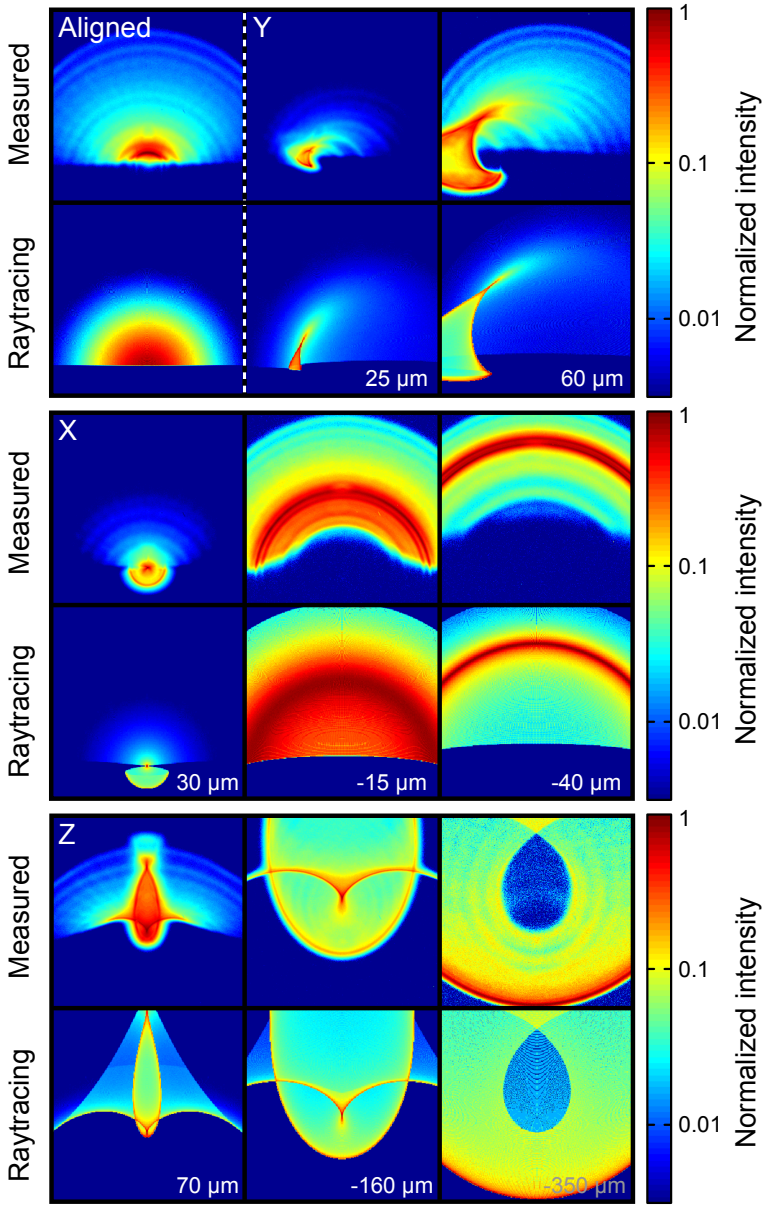


Figure 2.6: 2D CCD images when properly aligned (top row left) and for various misalignments in y (top row right) x (second row) and z (bottom row). Under each measured image the corresponding raytracing image is shown. For x and y the absolute misalignment is estimated by matching the raytracing images to the measurements. Absolute position values from the SEM stage were used for z.

the piezomotors accordingly to achieve a fully aligned system (see Fig. 2.6). For an experienced user this alignment procedure is straightforward and can be finished easily within 15 minutes, even if the initial misalignment varies due to non-reproducibility of mounting the piezosystem in the SEM. A next step is to automate the alignment procedure, which was beyond the scope of this project.

2.4 Measuring in k-space with a pinhole scanner

In the angular collection scheme as shown in Fig. 2.4 we have good angular precision but the wavelength selectivity is determined by the spectral filters which in our case have a bandwidth of 40 nm. For many nanophotonic systems, such as those supporting plasmonic resonances, this is not a problem because the spectral features are usually quite broad. However, to study high-Q cavities or periodic/aperiodic photonic crystals with a complex dispersion relation, it would be desirable to have much higher spectral resolution (ideally down to ~1 nm). Using spectral bandpass filters is impractical for this purpose. Therefore we have

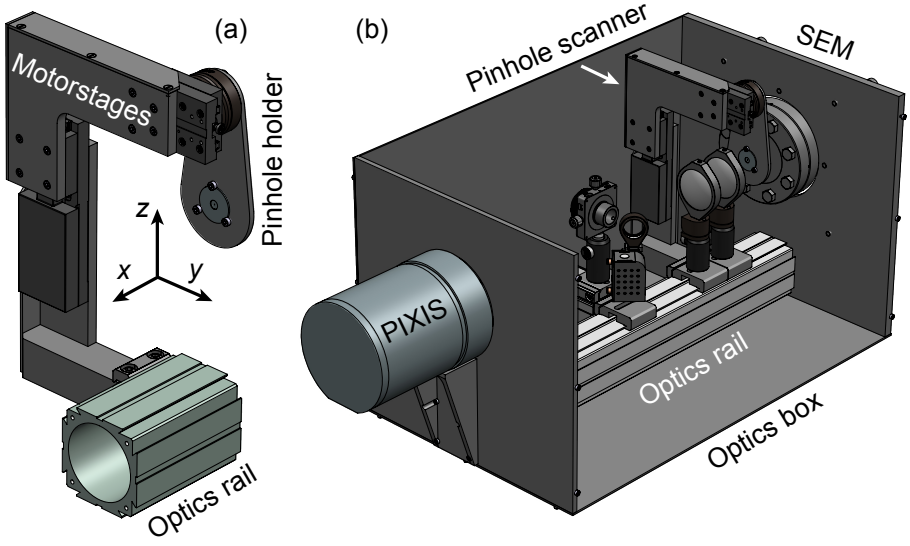


Figure 2.7: (a) Pinhole scanner design. The position of the motor stages and pinhole are indicated. For reference we have included the coordinate system. The scanner is clamped to the optics rail which is aligned with the optical axis of the parabolic mirror. (b) Implementation of the pinhole scanner in the optics box. The position of the SEM is indicated (also see Fig. 2.4(a) to see how the optics box is attached to the SEM). In this image the PIXIS 2D camera has been moved to the outside of the box to create more space for additional optics. (Images and design by Iliya Cerjak)

designed a complementary detection system similar to the system developed by Yamamoto *et al.* [106, 107]. It is based on a 2D pinhole scanner which acts as a filter in momentum-space. By choosing the pinhole size one can find the ideal tradeoff between signal level and angular resolution. Pinholes with 100, 150, and 500 μm diameter can be used. If we include the demagnification factor the collection area of a 4 × 4 binned CCD pixel of the 2D PIXIS camera is equivalent to a pinhole with a diameter of 117 μm. The smallest pinhole size thus roughly corresponds to one binned CCD pixel. After the pinhole one can use the spectrometer to measure the momentum-filtered spectrum with 1 nm spectral resolution for a broad wavelength range determined by the type of diffraction grating that is used in the spectrometer. In combination with the ability to very precisely locally excite a structure this allows for a new way of CL characterization. Although this measurement technique in principle is much slower than the angle-resolved detection scheme as described in Section 2.2, in many cases the measurement time can be significantly reduced by taking advantage of symmetries in the structure.

A schematic drawing of the pinhole scanner is shown in Fig. 2.7(a). Fig. 2.7(b) shows how the scanner is implemented in the optics box which is attached to the SEM (see Fig. 2.4(a)). The pinhole scanner that we have designed can be inserted and removed mechanically from the beam path so one can easily switch between different measurement configurations. The pinhole movement is controlled by two motorized translation stages which allows pinhole scanning in the xz-plane with a minimum stepsize of 0.05 μm (bidirectional repeatability = 1.6 μm and a backlash < 6 μm). This is more than sufficient for precise angular measurements as these require a typical stepsize of ≥ 50 μm. The pinhole holder is large enough such that the rest of the beam is always blocked. The scanner geometry was designed by Iliya Cerjak. The pinhole scanning and camera data collection are synchronized through a software program developed by Sander van de Haar and Sjoerd Wouda, all at AMOLF.

2.5 Electron energy-loss spectroscopy

As described in Section 2.1 EELS is a technique that is complementary to CL. We have performed EELS experiments (Chapter 10) in a 300 keV abberation-corrected FEI Titan transmission electron microscope (Fig. 2.8(a)) located at the Nanocharacterization Laboratory at Stanford University (CA, USA). This TEM is equipped with an electron monochromator and Gatan EEL spectrometer in which electrons of different energies are separated by a magnetic field and subsequently imaged by a camera (Fig. 2.8(b)). The EELS measurements are performed in scanning transmission electron microscopy (STEM) mode where the electrons are focused to a spot of ~1 nm. During the EELS acquisition one can simultaneously collect a STEM image using the annular dark field detector (ADF) as the EELS spectrometer only collects electrons close to the beam normal.

With EELS one can study core transitions to spatially resolve the atomic com-

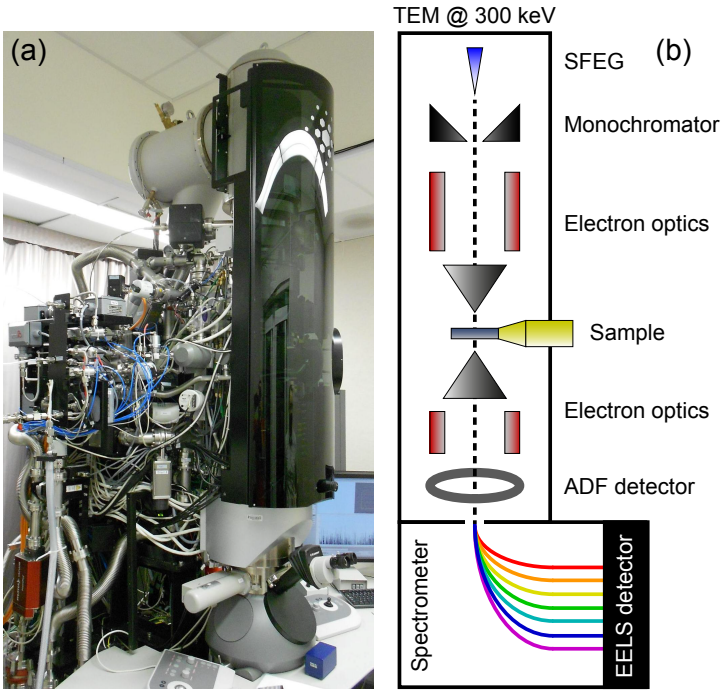


Figure 2.8: (a) Photograph of FEI Titan TEM at Stanford University (b) Schematic of the EELS setup. After interaction with the sample the electrons are separated in energy by a magnetic field. Subsequently the electron signal is converted to an optical signal by a phosphor screen and detected by a CCD camera.

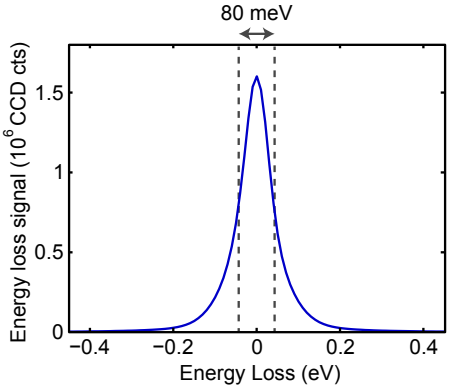


Figure 2.9: EELS spectrum showing zero-loss peak measured through a punctured membrane (vacuum) for 300 keV electron energy. The FWHM is indicated by the gray dashed lines (80 meV).

position of a structure [108]. The extreme sensitivity of this technique is apparent from the fact that atomic defects in graphene [109] or specific atom columns in crystals can be resolved for instance [110]. Usually these transitions involve high energies (typically > 100 eV) and as result the corresponding loss peaks are well separated from the primary beam energy and can be resolved quite easily. However, for EELS measurements in the visible/NIR spectral regime the energy-loss features are very close to the "zero-loss" peak (ZLP) of the primary beam. It is thus essential to minimize the energy width of the primary beam. State-of-the-art TEMs have efficient monochromators which allow for a very narrow energy distribution of the electrons in the beam. One can measure this distribution by measuring an EELS spectrum through a punctured TEM membrane (through vacuum). Such a measurement is shown in Fig. 2.9 for 300 keV electrons, measured using the Stanford TEM. Because there are no sample interactions only the zero-loss peak corresponding to the unperturbed primary beam is observed. In general, samples prepared for TEM are so thin that a large fraction of the electrons are transmitted without interacting with the sample and hence this ZLP is always clearly present in any EELS measurement. In this case we find a full-width half-maximum (FWHM) for the ZLP of 80 meV which is only 2.7×10^{-7} of the average electron energy, and good enough for resolving spectral features on the tail of the ZLP in the spectral region of interest.